Absolute differential cross sections for electron capture and loss by kilo-electron-volt hydrogen atoms

G. J. Smith, L. K. Johnson, R. S. Gao, K. A. Smith, and R. F. Stebbings
Department of Physics, Rice University, P.O. Box 1892, Houston, Texas 77251;
Department of Space Physics and Astronomy, Rice University, P.O. Box 1892, Houston, Texas 77251;
and Rice Quantum Institute, Rice University, P.O. Box 1892, Houston, Texas 77251
(Received 31 May 1991)

This paper reports measurements of absolute differential cross sections for electron capture and loss for fast hydrogen atoms incident on H_2, N_2, O_2, Ar, and He. Cross sections have been determined in the 2.0- to 5.0-keV energy range over the laboratory angular range 0.02°–2°, with an angular resolution of 0.02°. The high angular resolution allows us to observe structure at small angles in some of the cross sections. Comparison of the present results with those of other authors generally shows very good agreement.

PACS number(s): 34.70.+e, 34.50.Lf

I. INTRODUCTION

Charge-changing processes in kilo-electron-volt energy atomic collisions are of considerable importance in environments ranging from tokomak plasmas to planetary atmospheres. In this paper we report measurements of absolute differential cross sections (DCS's) for electron loss and electron capture by kilo-electron-volt energy hydrogen atoms in collisions with H_2, N_2, O_2, Ar, and He. The measured cross sections are for ground-state H projectiles having kinetic energies between 2 and 5 keV and are differential in laboratory scattering angle between 0.02° and 2°.

II. APPARATUS AND EXPERIMENTAL METHOD

Figure 1 shows a schematic of the apparatus, which has been previously described in detail [1,2]. Positively charged ions emerging from the electron-impact ion source are accelerated to the desired energy and focused by an electrostatic lens. The resulting beam is momentum analyzed by a pair of bending magnets and enters a charge-transfer cell (CTC), where some of the fast protons are converted to fast neutral atoms via charge transfer with krypton gas. At the collision energies used in this work, near-resonant $H^+ + Kr$ charge transfer produces predominantly ground-state hydrogen. A strong electric field ($\sim$400 V/cm) applied between deflection plates DP1 removes ions from the beam and quenches any $2s$ metastable atoms present via Stark mixing of the $2s$ with the short-lived $2p$ state. The fraction of the atom beam reaching the target cell (TC) in an excited state is therefore insignificant. After passing through the TC, scattered atoms and product ions as well as unscattered primary atoms are collected on position-sensitive detectors (PSD's).

The high angular resolution is provided by apertures of 10 and 20 μm diameter at the exit of the CTC and the entrance to the TC, respectively. With the apertures separated by $\sim$19 cm, the atom beam is collimated to less than 0.005° divergence and has a flux of about 2000 to 2500 particles per second.

In the energy range 2–5 keV the cross sections for electron loss

$$H + X \rightarrow H^+ + X + e^- , \quad (1)$$

$$H + X \rightarrow H^+ + X^- \quad (2)$$

and electron capture

$$H + X \rightarrow H^- + X^+ \quad (3)$$

are generally small compared to those for neutralization

$$H^+ + X \rightarrow H + X^+ , \quad (4)$$

$$H^- + X \rightarrow H + X + e^- , \quad (5)$$

$$H^- + X \rightarrow H + X^- , \quad (6)$$

and it is necessary to adjust the experimental conditions to ensure a low probability that the charged products of

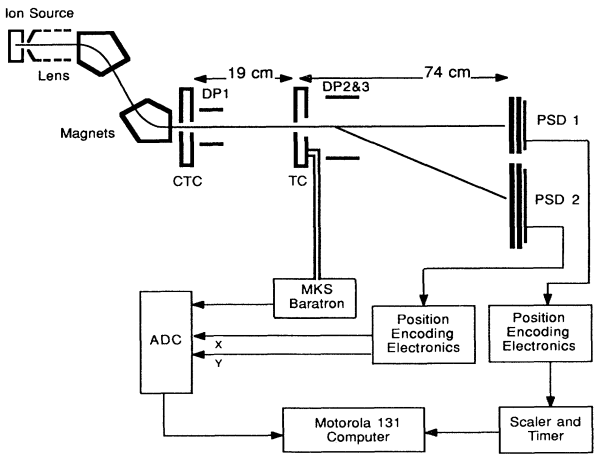

FIG. 1. Schematic of the apparatus.

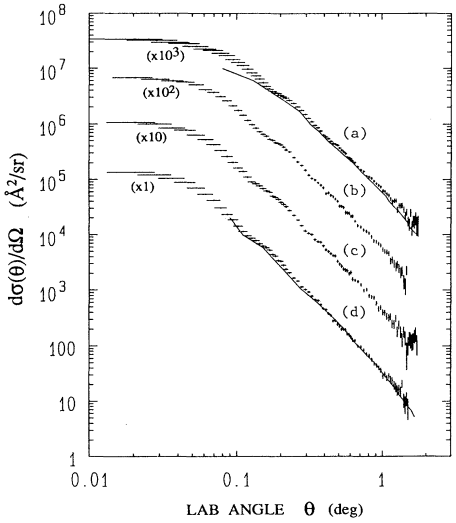

FIG. 2. DCS's for electron loss in $H+H_2$ collisions at (a) 2 keV, (b) 3 keV, (c) 4 keV, and (d) 5 keV. A comparison between the present data (+) and Fleischman, Barnett, and Ray (——, 2 and 5 keV) is shown. Note that the DCS values have been multiplied by the factors indicated on the figure.

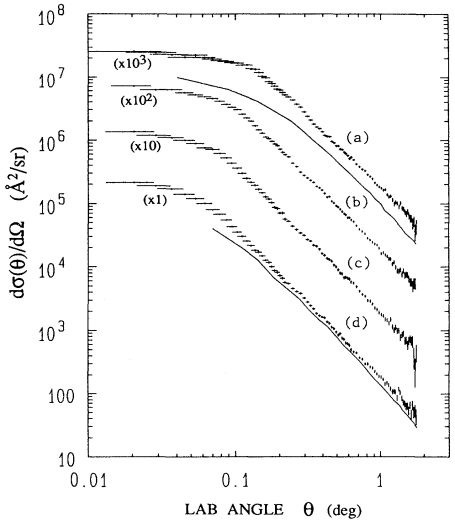

FIG. 4. DCS's for electron loss in $H+O_2$ collisions at (a) 2 keV, (b) 3 keV, (c) 4 keV, and (d) 5 keV. A comparison between the present data (+) and Fleischman, Barnett,and Ray (——, 2 and 5 keV) is shown. Note that the DCS values have been multiplied by the factors indicated on the figure.

reactions (1)–(3) will be subsequently reneutralized by reactions (4)–(6). To this end the pressure in the 2.6-mm-long target cell is typically maintained in the 10–20 mTorr range. In some instances measurements were made at several target-cell pressures to assess the importance of these secondary collisions of the product ions, and small ($<10\%$) corrections were made to the reported cross sections to account for such effects.

Scattered atoms and unscattered primary beam atoms are detected by a PSD with a 2.5-cm-diam active area which is axially located 74 cm beyond the TC (PSD1). The H^+ and H^- product ions are deflected through an angle of $\sim 5°$ by a pair of deflection plates (see Fig. 1, DP2 and DP3) and are detected on a second PSD with a

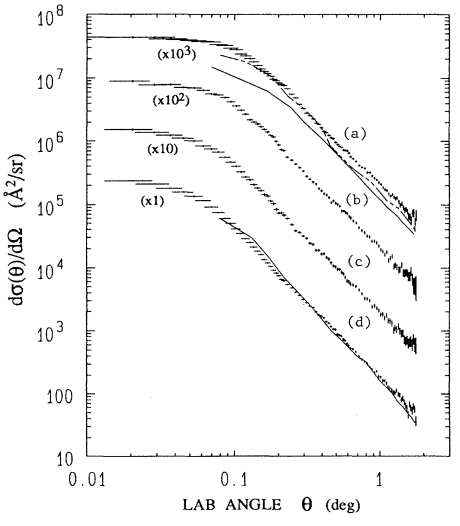

FIG. 3. DCS's for electron loss in $H+N_2$ collisions at (a) 2 keV, (b) 3 keV, (c) 4 keV, and (d) 5 keV. A comparison between the present data (+), Fleischman, Barnett, and Ray (——, 2 and 5 keV), and Cisneros *et al.* (----, 2 keV) is shown. Note that the DCS values have been multiplied by the factors indicated on the figure.

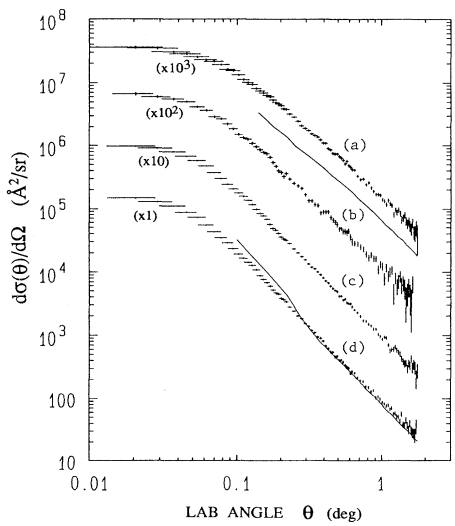

FIG. 5. DCS's for electron loss in H+Ar collisions at (a) 2 keV, (b) 3 keV, (c) 4 keV, and (d) 5 keV. A comparison between the present data (+) and Fleischmann, Barnett, and Ray (——, 2 and 5 keV) is shown. Note that the DCS values have been multiplied by the factors indicated on the figure.

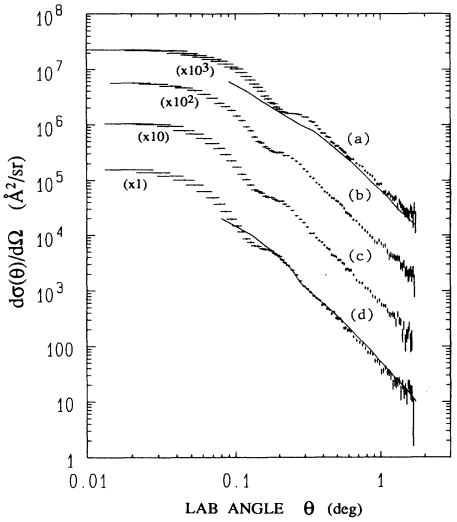

FIG. 6. DCS's for electron loss in H+He collisions at (a) 2 keV, (b) 3 keV, (c) 4 keV, and (d) 5 keV. A comparison between the present data (+) and Fleischman, Barnett, and Ray (——, 2 and 5 keV) is shown. Note that the DCS values have been multiplied by the factors indicated on the figure.

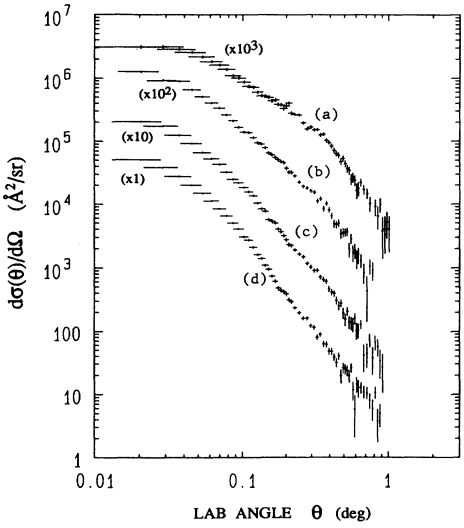

FIG. 8. DCS's for electron capture in H+N_2 collisions at (a) 2 keV, (b) 3 keV, (c) 4 keV, and (d) 5 keV. Note that the DCS values have been multiplied by the factors indicated on the figure.

4.0-cm-diam active area (PSD2), which is located off of the beam axis coplanar with PSD1. Details of the design and operation of the PSD's have been described in a previous paper [3]. To ensure that this deflection system does not introduce any significant distortion in the scattering pattern, the cross section for elastic scattering of He^+ by He, which had been previously measured [4] and found to have very pronounced structure, was reexamined. The scattering pattern observed with the present arrangement was found to be identical to that measured earlier where no deflection system was used. From this measurement it is concluded that the present measurements of electron capture and loss are free of apparatus-induced distortion. A Motorola MVME 131 computer monitors the outputs of the two PSD's, sorting the arrival coordinates of each particle detected on PSD2 into bins

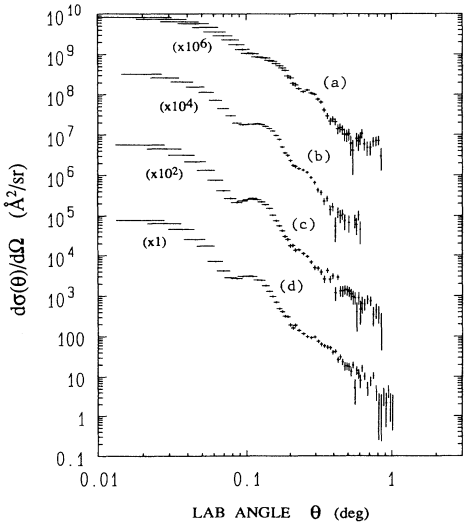

FIG. 7. DCS's for electron capture in H+H_2 collisions at (a) 2 keV, (b) 3 keV, (c) 4 keV, and (d) 5 keV. Note that the DCS values have been multiplied by the factors indicated on the figure.

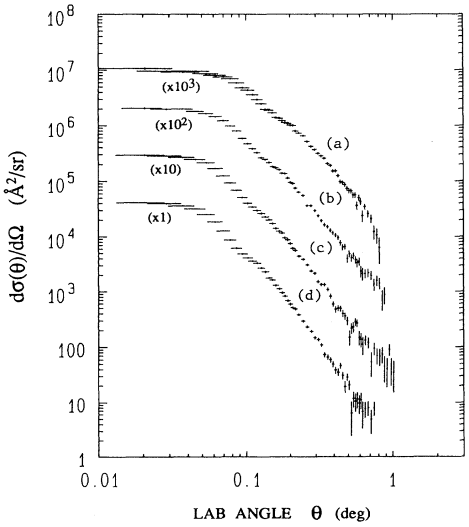

FIG. 9. DCS's for electron capture in H+O_2 collisions at (a) 2 keV, (b) 3 keV, (c) 4 keV, and (d) 5 keV. Note that the DCS values have been multiplied by the factors indicated on the figure.

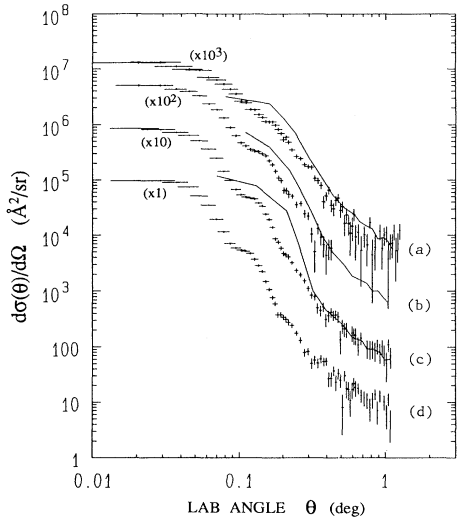

FIG. 10. DCS's for electron loss in H+Ar collisions at (a) 2 keV, (b) 3 keV, (c) 4 keV, and (d) 5 keV. A comparison between the present data (+) and Martinez *et al.* (——, 2, 3, and 4 keV) is shown. Note that the DCS values have been multiplied by the factors indicated on the figure.

in a 360×360 memory array and recording the total number of particles detected on PSD1. Each bin in the memory array corresponds to a 106×106-μm^2 area on the PSD surface. Although there are several factors contributing to each PSD's absolute detection efficiency, only the relative efficiency of the two PSD's is needed for an absolute cross-section measurement. Relative calibration of the PSD's is performed by deflecting an ion beam back and forth first to one PSD and then the other, taking care to accurately simulate the flux density and operating conditions each PSD experienced during data accumulation. This technique only determines the relative detection efficiency of the PSD's for ions. The PSD detection efficiencies for H^+, H^-, and H of the same energy are identical to within 5% in the energy range relevant to this experiment [5,6].

Under the thin target conditions used in this experiment, the differential cross sections are determined from the measured quantities by the relation

$$\frac{d\sigma(\theta)}{d\Omega} = \frac{\Delta S(\theta)}{S_0 n l \Delta\Omega} , \tag{7}$$

where S_0 is the primary beam flux in particles per second, $\Delta S(\theta)$ is the flux scattered at an angle θ into a solid angle $\Delta\Omega$, l is the physical length of the cell, and n is the target gas number density obtained by measuring the gas pressure in the TC with a MKS Baratron capacitance manometer.

Measurement of the scattered flux $\Delta S(\theta)$ requires that one distinguish between counts due to scattering in the target cell and background counts arising from other sources such as large-angle direct scattering of the primary atoms onto the ion detector, scattering from the apertures, and random detector noise. This is accomplished by collecting two sets of data, the first with the product ions deflected onto PSD2 (signal on) and the second with the ions deflected away from the detectors (signal off). In this procedure, the gas was always present in the target cell. Subsidiary experiments showed that, after a small correction was made for reneutralization of the product ions by secondary collisions in the cell, the amount of signal measured was a linear function of target cell pressure and that there was no H^+ or H^- signal present in the absence of target gas. The scattered flux $\Delta S(\theta)$ is then determined by organizing the two-dimensional array into concentric rings about the scattering center and subtracting the signal-off data from the signal-on data. This process is performed once for the

TABLE I. Experimental uncertainties affecting cross-section amplitude and angle.

Amplitude effects	Uncertainty
Counting statistics	2%
PSD operating point	2%
PSD calibration	1%
TC length l	2%
Secondary collision correction	1%
TC pressure (number density n)	1%
Baratron thermal transpiration	2%
Neutral-ion detection efficiency	5%
Angular effects	
TC to PSD distance	1%
Beam divergence	0.005°
Analysis ring width (106 μm)	0.008°
PSD position encoding error[a]	0.008°

[a]Reference [1].

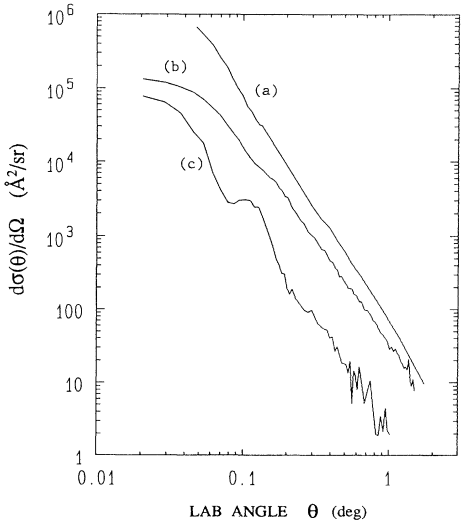

FIG. 11. Comparison of DCS's for (a) direct scattering, (b) electron loss, and (c) electron capture in H(5 keV)+H_2 collisions.

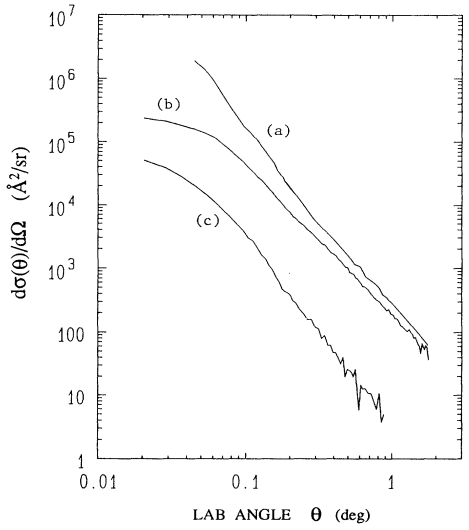

FIG. 12. Comparison of DCS's for (a) direct scattering, (b) electron loss, and (c) electron capture in H(5 keV)+N_2 collisions.

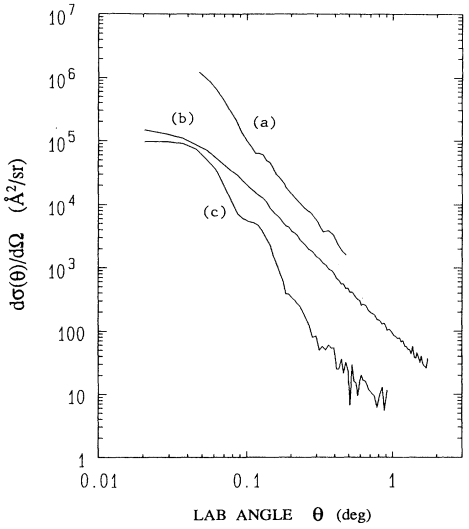

FIG. 14. Comparison of DCS's for (a) direct scattering, (b) electron loss, and (c) electron capture in H(5 keV)+Ar collisions.

H^+ measurement and again for the H^- measurement. The experimental uncertainty in the number of counts at a given angle is primarily statistical, while the angular uncertainties arise from the finite width of the primary atom beam, the discrete nature of the analysis rings, and inherent electronic errors in the detector's position encoding circuits. These uncertainties are shown in Figs. 2–10 as vertical and horizontal error bars. Other factors that add uncertainty to the measurement are summarized in Table I.

III. RESULTS AND DISCUSSION

Differential electron-capture and -loss cross sections determined in the present work are presented in Figs. 2–10. The electron capture data show some structure in the DCS's. That is presumably due either to curve crossings of the potential-energy surfaces for the initial and final states or to Demkov-type oscillations in the electron capture probability as a function of scattering angle. The electron-loss cross sections for He and H_2 targets also show pronounced structure. That is difficult to explain if the lost electron undergoes a direct transition to the con-

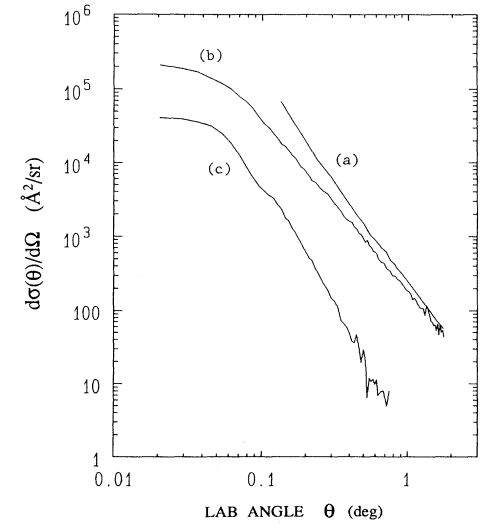

FIG. 13. Comparison of DCS's for (a) direct scattering, (b) electron loss, and (c) electron capture in H(5 keV)+O_2 collisions.

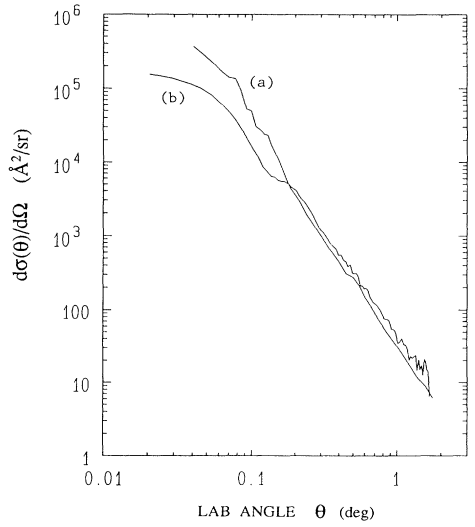

FIG. 15. Comparison of DCS's for (a) direct scattering and (b) electron loss in H(5 keV)+He collisions.

tinuum, and it may point to the involvement of intermediate excited states in the electron loss process.

Comparisons of the present differential measurements with those of other investigators are shown in Figs. 2–6 and 10. Electron-loss cross-section comparisons with Fleischmann, Barnett, and Ray [7] generally show good agreement, particularly at 5.0 keV. At 2.0 keV, there is still good agreement between the slopes of the two measurements, although the magnitude of the measurements sometimes differ. This is not too disturbing, however, since Fleischmann, Barnett, and Ray measured relative cross sections and normalized to several other investigators' total cross sections, which tend to vary from author to author. Comparisons with Cisneros *et al.* [8] and Martinez *et al.* [9] also show reasonably good agreement at the high end of the angular range. At very small angles the agreement is worse. However, the Cisneros and Martinez data are less specific in this range due to their limited angular resolution.

It is also interesting to compare the direct scattering [10–12], electron-loss, and electron-capture DCS's for a given set of reactants, as seen in Figs. 11–15. In carrying out their electron-loss measurements, Van Zyl *et al.* [13] assert that the functional forms of the direct scattering and electron-loss differential cross sections (with respect to angle) are similar, except at very small angles. The present results generally support this assertion at angles greater than about 0.2°. It is also notable that the electron-capture cross sections tend to be more strongly forward peaked, implying that only a small percentage of the total cross section lies beyond the measured angular range.

Comparison of the present as well as previous measurements with theoretical predictions would be both interesting and informative. However, the few calculations [14,15] that have been made for these processes show unsatisfactory agreement with experimental data in the low kilo-electron-volt energy range.

ACKNOWLEDGMENTS

This work was supported by the Robert A. Welch Foundation, NASA, and the NSF Atmospheric Sciences section.

[1] D. E. Nitz, R. S. Gao, L. K. Johnson, K. A. Smith, and R. F. Stebbings, Phys. Rev. A **35**, 4541 (1987).
[2] R. S. Gao, L. K. Johnson, D. E. Nitz, K. A. Smith, and R. F. Stebbings, Phys. Rev. A **36**, 3077 (1987).
[3] R. S. Gao, P. S. Gibner, J. H. Newman, K. A. Smith, and R. F. Stebbings, Rev. Sci. Instrum. **55**, 1756 (1984).
[4] R. S. Gao, L. K. Johnson, D. A. Schafer, J. H. Newman, K. A. Smith, and R. F. Stebbings, Phys. Rev. A **38**, 2789 (1988).
[5] L. K. Johnson, R. S. Gao, C. L. Hakes, K. A. Smith, and R. F. Stebbings, Phys. Rev. A **40**, 4920 (1989).
[6] R. S. Gao, L. K. Johnson, G. J. Smith, C. L. Hakes, K. A. Smith, N. F. Lane, R. F. Stebbings, and M. Kimura, Phys. Rev. A **44**, 5599 (1991).
[7] H. H. Fleischmann, C. F. Barnett, and J. A. Ray, Phys. Rev. A **10**, 569 (1974).
[8] C. Cisneros, I. Alvarez, C. F. Barnett, and J. A. Ray, Phys. Rev. A **14**, 84 (1976).
[9] H. Martinez, A. Morales, J. De Urquijo, I. Alvarez, and C. Cisneros, Nucl. Instrum. Methods B **40/41**, 44 (1989).
[10] J. H. Newman, Y. S. Chen, K. A. Smith, and R. F. Stebbings, J. Geophys. Res. **91**, 8947 (1986).
[11] L. K. Johnson, R. S. Gao, K. A. Smith, and R. F. Stebbings, Phys. Rev. A **38**, 2794 (1988).
[12] R. S. Gao, L. K. Johnson, K. A. Smith, and R. F. Stebbings, Phys. Rev. A **40**, 4914 (1989).
[13] B. Van Zyl, T. Q. Le, H. Neumann, and R. C. Amme, Phys. Rev. A **15**, 1871 (1977).
[14] H. Levy II, Phys. Rev. **185**, 7 (1969).
[15] D. R. Bates and A. Williams, Proc. Phys. Soc. London Sect. A **70**, 306 (1957).